Field-induced barrier penetration in the quartic potential

L. E. Reichl and W. M. Zheng
Center for Studies in Statistical Mechanics, University of Texas at Austin, Austin, Texas 78712
(Received 6 September 1983)

The problem of a particle trapped in a quartic double-well potential in the presence of a monochromatic external field is studied. Renormalization-group techniques are used to determine at what external field frequencies and amplitudes barrier penetration can occur for a particle initially trapped at a given energy in one of the potential wells.

I. INTRODUCTION

A problem of great current interest concerns the mechanism by which a dynamic external field might destabilize systems by increasing the rate of transition over potential barriers on the microscopic level. In this paper, we consider the simplest possible model system which contains the essential features of this problem—namely, that of a particle trapped in a quartic (double-well) potential in the presence of a monochromatic external force field. As we shall show for this system, predictions can be made analytically for the external field amplitude (at a given frequency) necessary to open a pathway through the phase space which will enable a particle of a given energy to escape one of the potential wells.

As has been discussed elsewhere,[1] a dynamic external field induces a dense set of resonance zones in the phase space of a conservative system. For weak external fields, the overall behavior of these induced resonance zones is largely determined by properties of the unperturbed system and will be dominated by a set of principle resonance zones. For very weak external fields, the principle resonance zones remain isolated. A particle in the vicinity of one principle resonance zone cannot travel through the phase space to the vicinity of a neighboring principle zone. However, as the amplitude increases, the KAM (Kolmogorov-Arnol'd-Moser) invariants in the region between the two principle zones begin to be destroyed until a pathway is finally opened between the two zones and the phase space begins to appear chaotic (from now on we shall call this process "breakdown").

A very simple criterion for determining when breakdown (often called "overlap") occurs has been described by Chirikov.[2,3] However, recently a more accurate method was developed by Escande and Doveil[4] using renormalization-group techniques. We shall adapt the renormalization-group techniques to the problem of barrier penetration which we consider here.

We begin in Sec. II with a discussion of the properties of a quartic double-well system in the absence of an external field. These properties determine the location and size of the induced principle resonance zones when the dynamic external field is present. In Sec. III we describe the behavior of the induced primary resonance zones when an external field is present and in Sec. IV we introduce the two-resonance approximation and write the Hamiltonian in so-called "standard form" for application of the normalization group. In Sec. V, we give predictions for field-induced barrier penetration as a function of field frequency and amplitude and we compare some of these predictions to the results of numerical simulation. Finally, in Sec. VI we make some concluding remarks.

II. UNPERTURBED DOUBLE-WELL SYSTEM

We will first consider a particle of mass $m=2$ constrained to move along the x axis in a double-well potential

$$V(x)=-2x^2+x^4 . \tag{2.1}$$

The Hamiltonian for this system is

$$H=\tfrac{1}{4}p^2-2x^2+x^4=E_0 , \tag{2.2}$$

where E_0 is the total energy of the system and p and x are the momentum and position, respectively, of the particle. The potential $V(x)$ is plotted in Fig. 1. When $E_0<0$, the particle is trapped in one of the wells. When $E_0>0$, the particle is free to move across the barrier. The phase-space trajectories for this system for five different energies are plotted in Fig. 2. At energy $E_0=-1$ the system has two stable fixed points ($p=0$ and $x=\pm 1$) and at energy $E_0=0$ it has one unstable fixed point ($p=0$ and $x=0$).

We may perform a canonical transformation to new

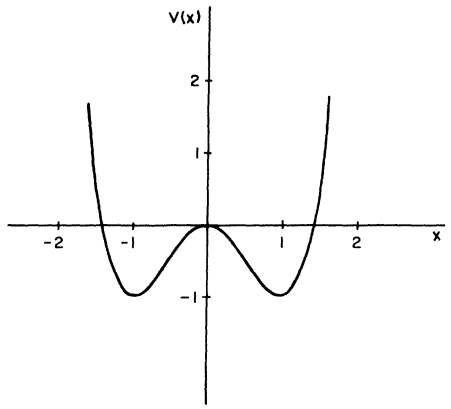

FIG. 1. Plot of quartic potential $V(x)=-2x^2+x^4$.

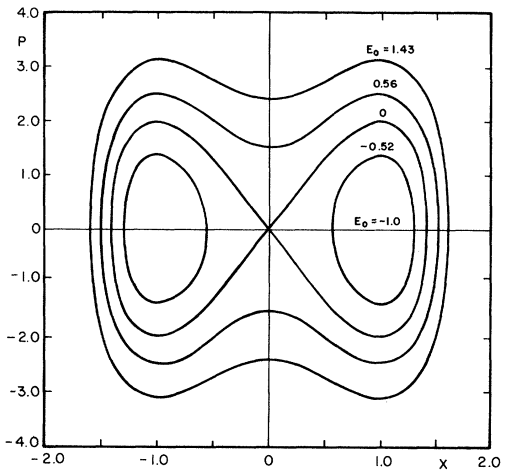

FIG. 2. Plot of phase-space trajectories for particle of mass $m=2$ trapped in the quartic potential $V(x)=-2x^2+x^4$. Trajectories are plotted for energies $E_0=-1$, -0.52, 0.0, 0.56, and 1.43. The trajectory $E_0=0.0$ is the separatrix and separates trapped motion from untrapped motion.

variables (J,ϕ) such that ϕ is cyclic.[5] The canonical transformation is

$$x=\sqrt{J+1}\,\mathrm{dn}\left[\frac{\phi}{\sqrt{2J}\,k},k\right] \tag{2.3}$$

and

$$p=-4J\,\mathrm{cn}\left[\frac{\phi}{\sqrt{2J}\,k},k\right]\mathrm{sn}\left[\frac{\phi}{\sqrt{2J}\,k},k\right], \tag{2.4}$$

where dn, cn, and sn are Jacobi elliptic functions and the modulus k is defined as

$$k^2=\frac{2J}{J+1}\ . \tag{2.5}$$

Note that when $E_0>0$, $k>1$ and Eqs. (2.3) and (2.4) can also be written as

$$x=\sqrt{J+1}\,\mathrm{cn}\left[\frac{\phi}{\sqrt{2J}},\frac{1}{k}\right] \tag{2.6}$$

and

$$p=-\frac{4J}{k}\,\mathrm{sn}\left[\frac{\phi}{\sqrt{2J}},\frac{1}{k}\right]\mathrm{dn}\left[\frac{\phi}{\sqrt{2J}},\frac{1}{k}\right]. \tag{2.7}$$

In terms of these new canonical variables, the Hamiltonian becomes

$$H=J^2-1=E_0\ . \tag{2.8}$$

The canonical variables (J,ϕ) are not action-angle variables.

III. PERTURBED DOUBLE-WELL SYSTEM

Let us consider next the motion of a particle of mass m in a more general double-well potential and in the presence of an oscillatory force field. The Hamiltonian can be written

$$\tilde{H}=\tilde{p}^2/2m-2B\tilde{x}^2+A\tilde{x}^4+\epsilon\tilde{x}\cos(\omega\tilde{t})\ , \tag{3.1}$$

where B and A are parameters which may be used to adjust the shape of the potential, ϵ and ω are the amplitude and frequency, respectively, of the external field, $\tilde{p}$ is the momentum of the particle, $\tilde{x}$ is its position, and $\tilde{t}$ is the time. We can now rescale variables, i.e., let

$$H=A\tilde{H}/B^2,\quad p=(2A/mB^2)^{1/2}\tilde{p},\quad x=(A/B)^{1/2}\tilde{x}\ ,$$

and $t=(2B/m)^{1/2}\tilde{t}$ and write the Hamiltonian in the form

$$H=\tfrac{1}{4}p^2-2x^2+x^4+\bar{\epsilon}x\cos(\bar{\omega}t)\ , \tag{3.2}$$

where $\bar{\epsilon}=\epsilon(A/B^3)^{1/2}$ and $\bar{\omega}=\omega(m/2B)^{1/2}$. Note that the equation of motion for x is just the Duffing equation.[6,7]

Hamiltonian (3.2) can be written in terms of canonical variables (J,ϕ) [cf. Eqs. (2.3) and (2.4)]. It then takes the form

$$H=J^2-1+\bar{\epsilon}\sqrt{J+1}\cos(\bar{\omega}t)\mathrm{dn}\left[\frac{\phi}{\sqrt{2J}\,k},k\right]. \tag{3.3}$$

Since the Jacobi elliptic functions are periodic, the Hamiltonian (3.3) may be expanded in a Fourier series. For $E_0<0$ it takes the form

$$H=J^2-1+\bar{\epsilon}\sum_{n=-\infty}^{\infty}g_n(J)\cos\left[\frac{n\pi\phi}{\sqrt{2J}\,kK(k)}-\bar{\omega}t\right], \tag{3.4}$$

where

$$g_n(J)=\frac{\pi}{\sqrt{2}(2-k^2)^{1/2}K(k)}\,\mathrm{sech}\left[\frac{|n|\pi K'(k)}{K(k)}\right] \tag{3.5}$$

and for $E_0>0$ it takes the form

$$H=J^2-1+\bar{\epsilon}\sum_{n=-\infty}^{\infty}h_n(J)\cos\left[\frac{(n+\frac{1}{2})\pi\phi}{\sqrt{2J}\,\bar{K}(k)}-\bar{\omega}t\right], \tag{3.6}$$

where

$$h_n(J)=\frac{\pi\sqrt{2J}}{2k\bar{K}(k)}\,\mathrm{sech}\left[\frac{(|n|+\frac{1}{2})\pi\bar{K}'(k)}{\bar{K}(k)}\right]. \tag{3.7}$$

In Eqs. (3.4)–(3.7), $K(k)$ is the complete elliptic integral of the first kind,

$$K'(k)=K[(1-k^2)^{1/2}],\quad \bar{K}=K\left[\frac{1}{k}\right],$$

and

$$\bar{K}'=K\left[\left[1-\frac{1}{k^2}\right]^{1/2}\right].$$

As can be seen from Eqs. (3.4) and (3.6), the external field introduces an infinite number of primary resonance zones into the phase space of this system. (See Ref. 1 for a more extensive discussion for the case of the Toda system.) For small $\bar{\epsilon}$, the primary resonances are located at values of $J\equiv J_n^c$ which satisfy the equations (for $E_0<0$)

$$\dot{\phi}=\frac{\bar{\omega}Kk\sqrt{2J}}{n\pi}=2J \tag{3.8}$$

and the equations (for $E_0 > 0$)

$$\dot{\phi} = \frac{\bar{\omega} K \sqrt{2J}}{(n+\frac{1}{2})\pi} = 2J \ . \tag{3.9}$$

A plot of J_n^c vs $\bar{\omega}$ is given in Fig. 3 for several values of n. These curves locate the position of the primary resonance zones in the phase space. The primary resonance zones are induced into the phase space by the external field. They are always spaced an equal distance apart along the frequency axis. As frequency is lowered the resonance zones in regions $J > 1$ and $J < 1$ all converge to $J = 1$.

IV. TWO-RESONANCE APPROXIMATION

We are interested in values of the external field amplitude $\bar{\epsilon}$ at which a particle which is initially trapped in one of the wells can be driven over the barrier. The smallest value of $\bar{\epsilon}$ at which this can occur will vary with frequency $\bar{\omega}$ of the external field. As we shall see, we can obtain fairly good estimates using the two-resonance approximation and renormalization-group techniques.

Let us focus on the region of phase space between resonance zones n_0 and n_0+1 for $E_0 < 0$. The Hamiltonian can then be written as

$$H = J^2 - 1 + \bar{\epsilon} g_{n_0}(J) \cos\left[\frac{n_0 \pi \phi}{\sqrt{2J}\, \kappa K(\kappa)} - \bar{\omega} t\right] + \bar{\epsilon} g_{n_0+1}(J) \cos\left[\frac{(n_0+1)\pi\phi}{\sqrt{2J}\, \kappa K(\kappa)} - \bar{\omega} t\right] . \tag{4.1}$$

This approximation will be good in the region $J_{n_0}^c < J < J_{n_0+1}^c$ and ϵ small.

It is now useful to make a canonical transformation to new coordinates $(\bar{p}_0, \bar{x}_0)$ in such a way that the point $\bar{p}_0 = 0$ is located at $J = J_{n_0}^c$ (we will shift the origin of coordinates and rescale them). Furthermore, the resonance zone n_0 will be at rest in this new reference frame. This can be accomplished by means of the generating function[8]

$$F(J, \bar{x}_0, t) = -(\bar{x}_0 - \bar{\omega} t) \int_{J_n^c}^{J} dJ' \frac{(2J')^{1/2} \kappa(J') K(J')}{n_0 \pi} \ . \tag{4.2}$$

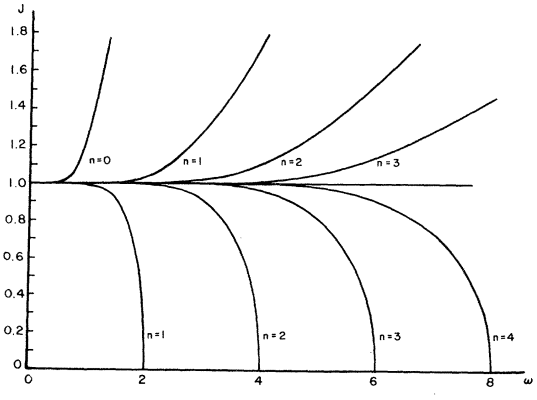

FIG. 3. Location of principle resonance zones as a function of frequency $\bar{\omega}$ and momentum J. Only the first four zones for energies $E_0 > 0$ and $E_0 < 0$ are plotted.

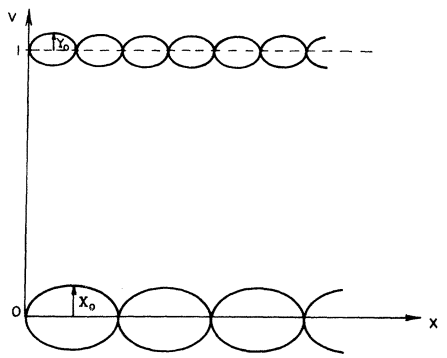

FIG. 4. A sketch of the phase space in the two-resonance approximation for a Hamiltonian in standard form. The zone of width $X_0 = 2(U_0^{(x)}/m_0)^{1/2}$ in velocity space has speed $v_0 = 0$ and zone of width $Y_0 = 2(U_0^{(y)}/m_0)^{1/2}$ has speed $v_0 = 1$.

The coordinates (J, ϕ) and $(\bar{p}_0, \bar{x}_0)$ are related through the equations

$$\bar{p}_0 = -\frac{\partial F}{\partial \bar{x}_0} = \int_{J_{n_0}^c}^{J} dJ' \frac{(2J')^{1/2} \kappa(J') K(J')}{n_0 \pi} \ , \tag{4.3}$$

where $\kappa_c = \kappa(J_{n_0}^c)$ and $K_c = K(\kappa_c)$, and

$$\phi = -\frac{\partial F}{\partial J} = (\bar{x}_0 - \bar{\omega} t) \frac{\sqrt{2J}\, \kappa K}{n_0 \pi} \ . \tag{4.4}$$

If we Taylor expand Eq. (4.3) about $J_{n_0}^c$ and revert the series, we find

$$J = J_{n_0}^c + \frac{n_0 \pi \bar{p}_0}{(2J_{n_0}^c)^{1/2} \kappa_c K_c} - \frac{n_0^2 \pi^2}{8 (J_{n_0}^c)^2 \kappa_c^2 K_c^3} \left[K_c + \frac{E_c}{1 - J_{n_0}^c}\right] \bar{p}_0^2 + \cdots \ , \tag{4.5}$$

where $E_c = E(\kappa_c)$ is the complete Jacobi elliptic integral of the second kind.

If we now make use of the resonance condition (3.8), and if we let $g_n(J) \to g_n(J_n^c)$ for $n = n_0$ and $n = n_0 + 1$, we

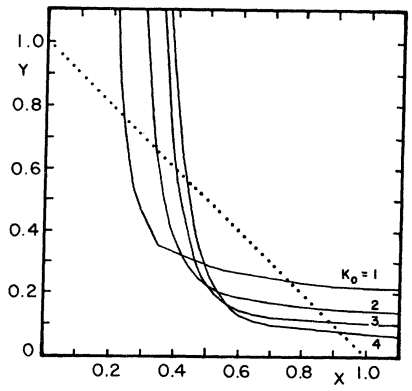

FIG. 5. Solid lines give renormalization-group predictions for breakdown. The dotted line gives the Chirikov prediction [redrawn from Ref. 4 (J. Stat. Phys.)].

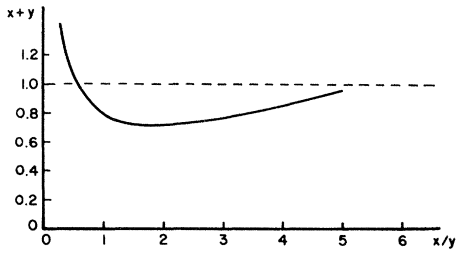

FIG. 6. Plot of breakdown criterion as function of X/Y and $X+Y$ for $k_0=2$. The dotted line is Chirikov; the solid line is the renormalization group.

obtain

$$H(\bar{p}_0,\bar{x}_0,t)=H+\frac{\partial F}{\partial t}$$
$$=(J^c_{n_0})^2-1-\frac{\bar{p}_0^2}{2m_0}+\bar{\epsilon}g_{n_0}(J^c_{n_0})\cos\bar{x}_0$$
$$+\bar{\epsilon}g_{n_0+1}(J^c_{n_0+1})\cos[k_0(\bar{x}_0-\Delta v_0 t)]\ . \quad (4.6)$$

The replacement $g_n(J)\rightarrow g_n(J^c_n)$ is necessary to best represent the relative sizes of the two resonance zones. In Eq. (4.6) we have introduced an effective mass,

$$m_0=\frac{2J^c_{n_0}k_c^2K_c^3}{n_0^2\pi^2[E_c/(1-J^c_{n_0})-K_c]}\ , \quad (4.7)$$

a wave vector,

$$k_0=\frac{n_0+1}{n_0}\ , \quad (4.8)$$

and the velocity of the resonance zone n_0+1,

$$\Delta v_0=\left[\frac{n_0}{n_0+1}-1\right]\bar{\omega}\ . \quad (4.9)$$

As a final step we will make a transformation to a coordinate frame in which resonance zone n_0+1 has unit velocity while the zone n_0 remains at rest. This can be accomplished by means of the canonical transformation $t_0=\Delta v_0 t$, $p_0=-\bar{p}_0/\Delta v_0$, $x_0=\bar{x}_0$, and $H_0=-H/(\Delta v_0)^2$. We then find

$$H_0(p_0,x_0,t_0)=\frac{[1-(J^c_{n_0})^2]}{(\Delta v_0)^2}+\frac{p_0^2}{2m_0}-U_0^{(x)}\cos x_0$$
$$-U_0^{(y)}\cos[K_0(x_0-t_0)]\ , \quad (4.10)$$

where

$$U_0^{(x)}=\frac{\bar{\epsilon}g_{n_0}(J^c_{n_0})}{(\Delta v_0)^2} \quad (4.11)$$

and

$$U_0^{(y)}=\frac{\bar{\epsilon}g_{n_0+1}(J^c_{n_0+1})}{(\Delta v_0)^2}\ . \quad (4.12)$$

A sketch of the system described by Hamiltonian (4.10) is given in Fig. 4. It consists of two resonance zones: one (n_0) with velocity $v_0=0$ and the other (n_0+1) with velocity $v_0=1$. The half-width of zone n_0 in velocity space is

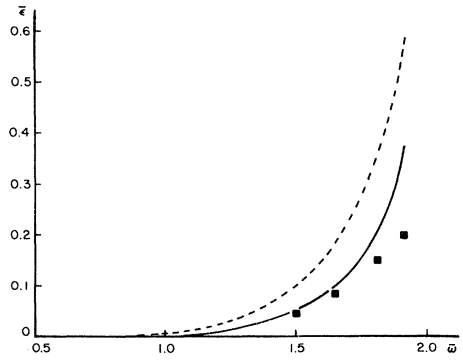

FIG. 7. Field amplitude at which breakdown occurs between primary zones $n_0=1$ and $n_0=2$ as a function of frequency. The dotted line is the Chirikov prediction. The solid line is the renormalization-group prediction. The squares give the result of numerical simulation.

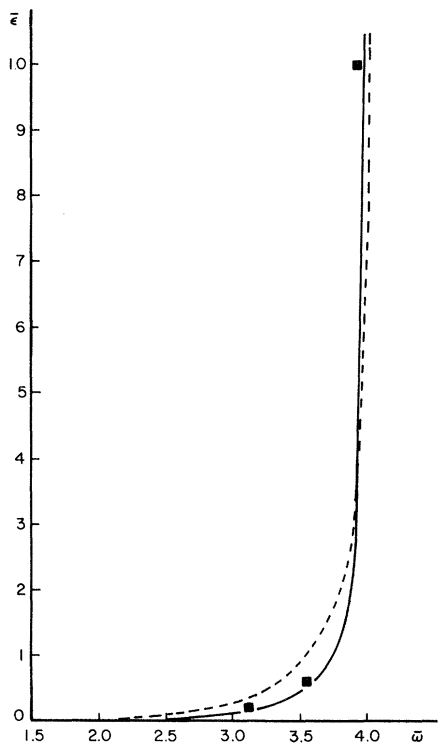

FIG. 8. Field amplitude at which breakdown occurs between primary zones $n_0=2$ and $n_0=3$ as a function of frequency. The dotted line is the Chirikov prediction. The solid line is the renormalization-group prediction. The squares give the result of numerical simulations. The point at $\bar{\epsilon}\approx 10$ only shows the order of magnitude of breakdown.

$$X_0=2\left[\frac{U_0^{(x)}}{m_0}\right]^{1/2} \tag{4.13}$$

and the half-width of zone n_0+1 in velocity space is

$$Y_0=2\left[\frac{U_0^{(y)}}{m_0}\right]^{1/2}. \tag{4.14}$$

The Hamiltonian (4.10) is now in standard form and is ready for application of the renormalization-group transformation.

V. RENORMALIZATION-GROUP ESTIMATES AND NUMERICAL RESULTS

The details of the renormalization-group transformation as applied to conservative dynamical systems has been discussed elsewhere.[4] We will apply the results of that method to the present problem. The renormalization-group analysis of the region between two given resonance zones gives a criterion for estimating the field amplitude at which breakdown (or overlap) occurs. The renormalization-group estimate improves considerably on the simpler Chirikov criterion as we shall see. The key results of Escande and Doveil are reproduced in Fig. 5. The dotted line gives the Chirikov criterion ($X_0+Y_0=1$) for breakdown. The solid lines give the renormalization-group results in the two-resonance approximation. That is, breakdown occurs when the sum X_0+Y_0 is equal to its value on one of the solid lines in Fig. 5. [Note that the particular curve that must be used depends on the value of k_0 Eq. (4.8)].

We will now obtain estimates for the amplitude $\bar{\epsilon}$ at which breakdown occurs between primary resonance zones $n_0=1$ and $n_0=2$ as a function of frequency $\bar{\omega}$ and we shall compare some of these estimates to numerical results. As we shall see, breakdown between zones $n_0\geq 2$ occurs at smaller amplitudes (for a given frequency) than that between zones $n_0=1$ and $n_0=2$. Thus, when breakdown between zones $n_0=1$ and $n_0=2$ occurs there is a finite probability for particles with energy within the region of influence of zones $n_0>1$ to cross the barrier.

First, we note that the resonance zone $n_0=1$ only exists for values of frequency $\bar{\omega}\leq 2$ (cf. Fig. 3), and that for $n_0=1$ we have $k_0=2$ [cf. Eq. (4.8)]. In Fig. 6 we have plotted the renormalization-group criterion for breakdown (solid curve) when $k_0=2$ as a function of the ratio X/Y vs $X+Y$. For a given ratio X/Y, breakdown (or overlap) will occur when $X+Y$ equals its value on the curve in Fig. 6. This information can be obtained from Fig. 5. Values of X_0 and Y_0 as a function of $\bar{\epsilon}$ and $\bar{\omega}$ are given by

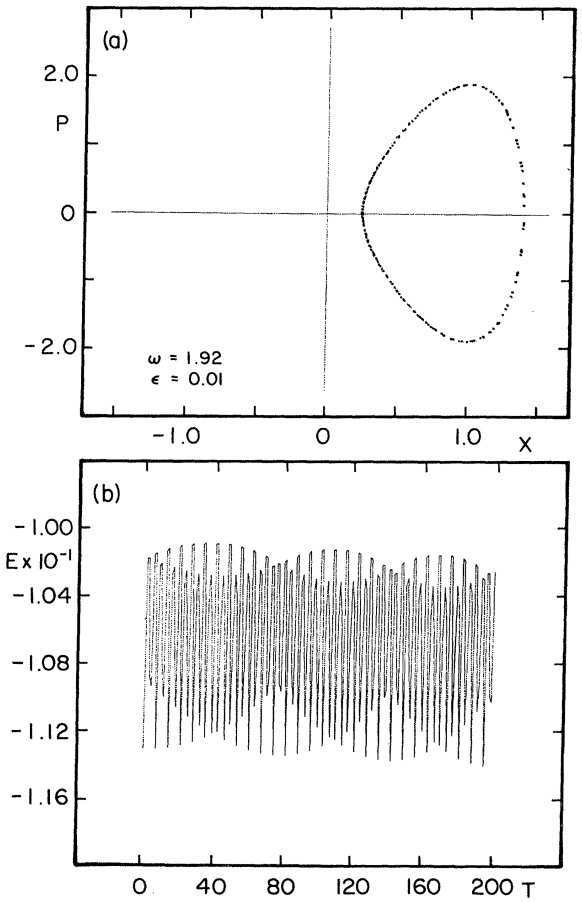

FIG. 9. (a) Strobe plot of p and x for $\bar{\omega}=1.92$ and $\bar{\epsilon}=0.01$. (b) Variation in energy of particle for $\bar{\omega}=1.92$ and $\bar{\epsilon}=0.01$.

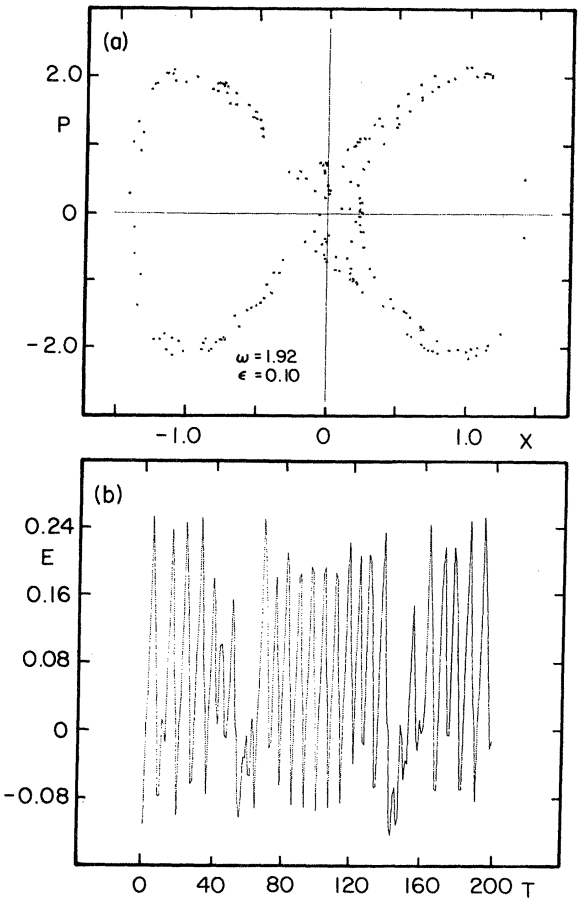

FIG. 10. (a) Strobe plot of p and x for $\bar{\omega}=1.92$ and $\bar{\epsilon}=0.10$. (b) Variation in energy of particle for $\bar{\omega}=1.92$ and $\bar{\epsilon}=0.10$.

$$X_0^2=\frac{2n_0^2(n_0+1)^2\bar{\epsilon}\pi^2 g_{n_0}(J_{n_0}^c)[K_c-E_c/(1-J_{n_0}^c)]}{\bar{\omega}^2 J_{n_0}^c \kappa_c^2 K_c^3} \tag{5.1}$$

and

$$Y_0^2=\frac{2n_0^2(n_0+1)^2\bar{\epsilon}\pi^2 g_{n_0+1}(J_{n_0+1}^c)[K_c-E_c/(1-J_{n_0}^c)]}{\bar{\omega}^2 J_{n_0}^c \kappa_c^2 K_c^3}, \tag{5.2}$$

where $\kappa_c^2=2J_{n_0}^c/(1+J_{n_0}^c)$, $E_c=E(\kappa_c)$, and $K_c=K(\kappa_c)$.

In Fig. 7 we give both the Chirikov and renormalization-group predictions for the external field amplitude $\bar{\epsilon}$ as a function of frequency $\bar{\omega}$, at which breakdown occurs between zones $n_0=1$ and $n_0=2$. We also give values of $\bar{\epsilon}$ observed in numerical simulation. We see that in all cases the renormalization-group estimates give better predictions than does the Chirikov estimate. We believe that the fairly large discrepancy between the experimental result and the prediction of the renormalization group to frequencies $\bar{\omega}=1.81$ and 1.91 may be due to a distortion in the $n_0=1$ zone caused by the nonresonant zone $n=-1$. As $n_0=1$ moves to larger values of J, this distortion effect should decrease.

In Fig. 8 we give the predictions for breakdown between $n_0=2$ and $n_0=3$. Again we see there is impressive agreement between the predictions of the renormalization group and the observed values.

In Figs. 9–14, we give the results of numerical simulation for amplitudes $\epsilon=0.01$, 0.10, 0.18, 0.20, 0.25, and 0.40 at frequency 1.92. At this frequency, $J_1^c=0.452$ and $J_2^c=0.997$. Thus, the region of influence of resonance zone $n_0=1$ is centered at $E_0=-0.796$ and the region of influence of resonance zone $n_0=2$ is centered at $E_0=-0.006$. In Figs. 9(a)–14(a) we give strobe plots of the momentum p and position x of the particle trapped in the bistable potential. That is, p and x are plotted each time the external field goes through one period of oscillation. In all cases, the particle starts with a momentum $p=0$ and position $x=0.24$ or with energy $E_0=-0.112$. Thus, the particle always starts with energy between the region of influence of resonance zones $n_0=1$ and $n_0=2$.

In Fig. 9 ($\bar{\epsilon}=0.01$) the external field has only a slight effect on the particle. We see that the particle energy oscillates between $E_0=-0.114$ and $E_0=-0.101$ and the particle never escapes the well. This also means that no particle with energy $E_0<-0.114$ can escape the well. In Fig. 10 ($\bar{\epsilon}=0.10$) we are starting to see the effect of the stochastic layer along the separatrix. All zones $n_0\geq 2$ have "broken down" and the region of phase space occu-

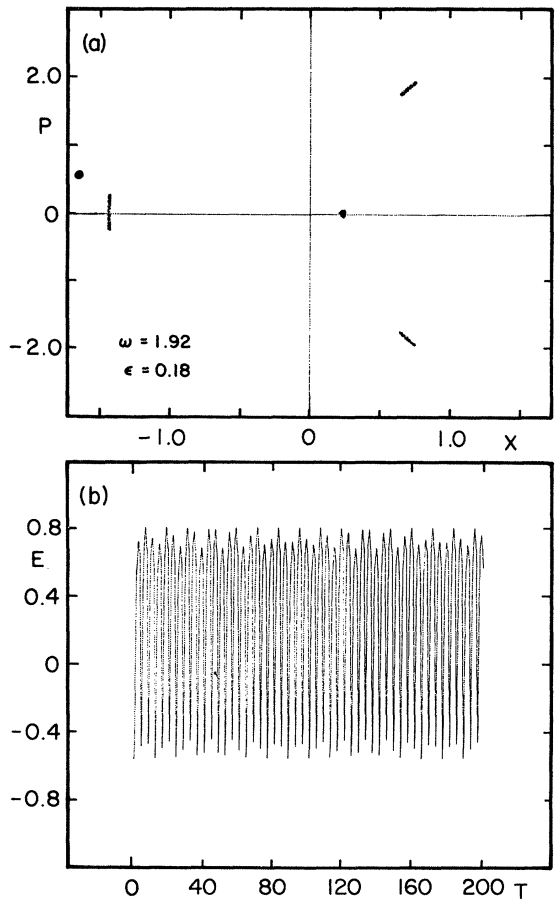

FIG. 11. (a) Strobe plot of p and x for $\bar{\omega}=1.92$ and $\bar{\epsilon}=0.18$. (b) Variation in energy of particle for $\bar{\omega}=1.92$ and $\bar{\epsilon}=0.18$.

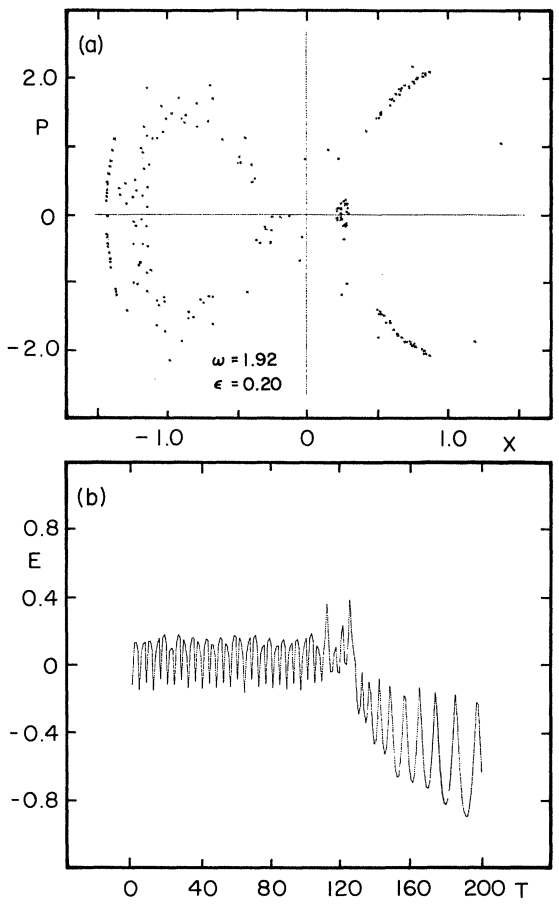

FIG. 12. (a) Strobe plot of p and x for $\bar{\omega}=1.92$ and $\bar{\epsilon}=0.20$. (b) Variation in energy of particle for $\bar{\omega}=1.92$ and $\bar{\epsilon}=0.20$.

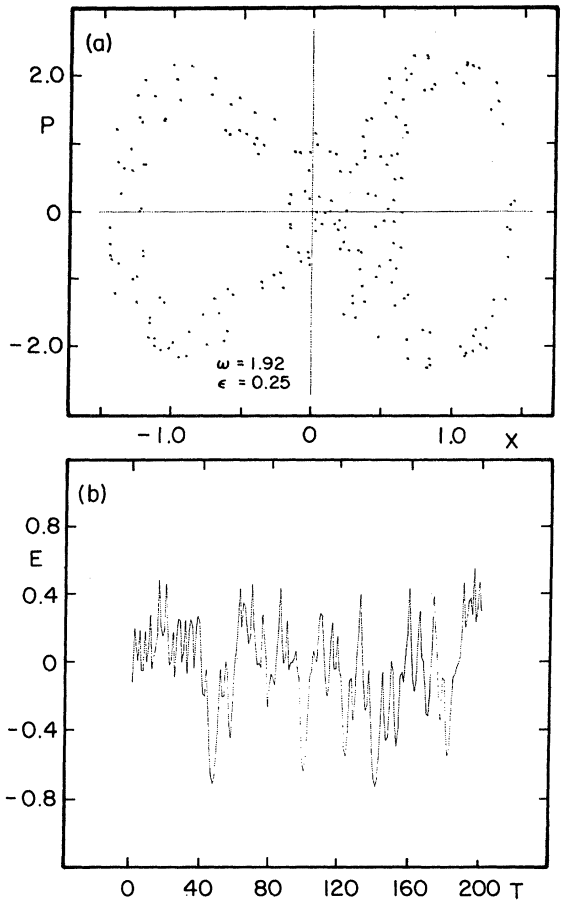

FIG. 13. (a) Strobe plot for p and x for $\bar{\omega}=1.92$ and $\bar{\epsilon}=0.25$. (b) Variation in energy of particle for $\bar{\omega}=1.92$ and $\bar{\epsilon}=0.25$.

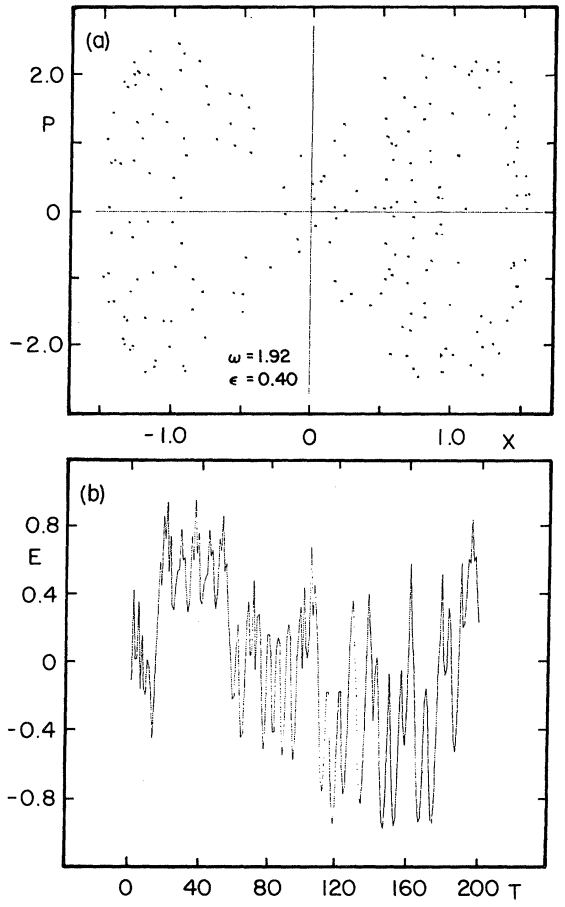

FIG. 14. (a) Strobe plot of p and x for $\bar{\omega}=1.92$ and $\bar{\epsilon}=0.40$. (b) Variation in energy of particle for $\bar{\omega}=1.92$ and $\bar{\epsilon}=0.40$.

pied by them has gone chaotic. At this value of $\bar{\epsilon}$ all particles with energy $E_0 > -0.13$ can escape the barrier. The energy of the particles oscillates between $E \approx -0.13$ and $E \approx +0.35$. Overlap between $n_0=1$ and $n_0=2$ has not occurred.

In Fig. 11 ($\bar{\epsilon}=0.18$) our particle becomes trapped in a quasiperiodic orbit which lies partly above the barrier and partly below it. In Fig. 12 ($\bar{\epsilon}=0.20$) we begin to see breakdown between $n_0=1$ and $n_0=2$. The particle not only can escape the barrier but it can also descend to energies $E_0 \approx -0.9$ and, therefore, the particle has made contact with resonance zone $n_0=1$. Conversely, there is a finite chance that any particle with energy $E_0 \gtrsim -0.9$ can escape the barrier. A pathway has been opened in the phase space for very low-energy particles to escape the barrier. In Figs. 13 ($\bar{\epsilon}=0.25$) and 14 ($\bar{\epsilon}=0.40$) we see the increasingly chaotic behavior and growing energy range sampled by the particle in the presence of the external field.

VI. CONCLUDING REMARKS

In this paper, we have presented a theory which enables us to predict the region of phase space in which trapped particles may be destabilized by a dynamic external field in the sense that a pathway will be opened in the phase space through which a fraction of the particles can migrate over the top of the potential barrier. We have studied here only those frequency domains near the low-energy natural frequencies of the unperturbed system. In all cases there is a critical field amplitude necessary to destabilize the system. We have found that the largest effect occurs near the frequency of the harmonic limit. [The harmonic limit of $V(x)$ is found by expanding $V(x)$ about the stable fixed points ($x=\pm 1$). The harmonic frequency is $\omega=2$.]

A problem of equal interest is the effect of very low-frequency fields (far below the harmonic limit) on this system. Because of the convergence of all resonance zones at very low frequencies, the potential exists for some effect at low frequencies. We shall discuss this problem in a subsequent paper.

ACKNOWLEDGMENTS

The authors wish to thank D. F. Escande for a very helpful discussion concerning the renormalization group and wish to thank R. de Fainchtein for help in obtaining adequate tables of elliptic integrals. L.E.R. wishes to thank the U.S. Air Force for partial support of this work through Contract No. F33615-78-D-0617 and W.M.Z. wishes to thank the Welch Foundation of Texas for partial support of this work.

[1]L. E. Reichl, R. de Fainchtein, T. Petrosky, and W. M. Zheng, Phys. Rev. A 28, 3051 (1983).
[2]V. Chirikov, Phys. Rep. 52, 263 (1979).
[3]See also L. H. Walker and J. Ford, Phys. Rev. 188, 416 (1969).
[4]D. F. Escande and F. Doveil, J. Stat. Phys. 26, 257 (1981); Phys. Lett. 83A, 307 (1981); Phys. Scr., T2, 126 (1982).
[5]H. Goldstein, *Classical Mechanics* (Addison-Wesley, Reading, Mass., 1950).
[6]G. Duffing, *Erzwungene Schwingungen bei veränderlicher Eigenfrequenz* (Braunschweig, Vieweg, 1918).
[7]H. T. Davis, *Introduction to Nonlinear Differential and Integral Equations* (Dover, New York, 1962).
[8]W. M. Zheng (unpublished).